

Optimised Design of a Printed Elliptical Spiral Antenna with a Dielectric Superstrate

S. K. Khamas and G. G. Cook

Dept. Electronic and Electrical Engineering, University of Sheffield,
Mappin St., Sheffield, S1 3JD, UK

Abstract – An elliptical spiral antenna embedded between a grounded dielectric substrate and superstrate is designed using a curved segment moment method employing complex images, which is driven by a marginal distribution optimisation algorithm. The spiral parameters together with substrate and superstrate permittivity and thickness values are optimised for low axial ratio and maximum gain and bandwidth. It is shown that the superstrate improves the bandwidth of the spiral.

I. INTRODUCTION

Spiral antennas can offer wide bandwidths, high efficiencies, squinted beams and circularly polarised radiation [1]. Previously the authors have developed a new Method of Moments (MoM) technique for the analysis of printed Archimedian, logarithmic and eccentric spirals that uses curved segmentation along the spiral arm, rather than the faceted approximations obtained with linear segmentation strategies, [2, 3]. The requirement of fewer curved segments gives the model a speed advantage which becomes increasingly important when the code may need to be run many times under an optimisation routine such as a Genetic Algorithm (GA) for example [4]. Printed spirals are useful as alternatives to patch antennas, and radomes can offer protection against the elements and also increase bandwidth. The authors have recently reported a curved segment analysis technique for embedded spiral design, employing the statistically based Optimisation using Marginal Distributions (OMD) technique to independently vary the permittivity and thickness of the dielectric substrate and superstrate for optimum axial ratio [5]. To expedite analysis a more efficient method is employed to calculate the Sommerfeld type potential functions required to compute the MoM impedance matrix. These Sommerfeld integrals are reformulated as closed-form complex image terms [6], whose coefficients are then evaluated using the Generalised Pencil of Functions (GPOF) technique [7].

Here we extend the analysis in [5] by applying it to an elliptical rather than Archimedian spiral, and also by optimising the spiral parameters in addition to the substrate and superstrate properties. Elliptical spirals can be used as conformal antennas and for tailoring radiation

patterns to specific requirements by altering the aspect ratio of the ellipse. Further, the spiral is also optimised for gain and bandwidth as well as axial ratio, and the effect of the superstrate on performance is considered.

II. THEORY

The theory presented here is intended to complement that in [5], so that only field equations which are specific to this particular spiral geometry are developed, to facilitate direct computation. A printed elliptical spiral is shown in Fig. 1a with a dielectric superstrate. In Fig. 1b, the electric field tangential to a thin wire contour ℓ located in a planar Cartesian co-ordinate frame by $\underline{\rho}(x, y)$ due to a current,

$$I_{\ell'} = I_n \frac{\sin(k(\Delta\ell' - |\ell' - \ell_n|))}{\sin(k\Delta\ell')} \quad (1)$$

at $\underline{\rho}(x', y')$ can be represented by, [8]

$$E_{\ell} = E_x \hat{\ell}_x + E_y \hat{\ell}_y = \frac{1}{j\omega\epsilon_2} \int_{\ell_{n-1}}^{\ell_{n+1}} I_{\ell'} k^2 G \left(\frac{\partial \rho_{x'}}{\partial \ell'} \frac{\partial \rho_x}{\partial \ell} + \frac{\partial \rho_{y'}}{\partial \ell'} \frac{\partial \rho_y}{\partial \ell} \right) + \frac{\partial I_{\ell'}}{\partial \ell'} \frac{\partial}{\partial \ell} (G + \Pi). \quad (2)$$

Where $k = 2\pi / \lambda$, $\omega = 2\pi f$, $\epsilon_2 = \epsilon_{r2}\epsilon_o$, $\epsilon_1 = \epsilon_{r1}\epsilon_o$ and $\Delta\ell'$ is the segment length. The terms G and Π are the potential (Green's) functions which couple sources to fields in the presence of planar layered dielectric media.

The MoM impedance matrix element linking curved source sinusoid n to curved test sinusoid m is then,

$$Z_{mn} = \frac{I}{\sin(k\Delta\ell)} \left[\int_{\ell_{m-1}}^{\ell_{m+1}} \sin(k(\Delta\ell - |\ell - \ell_m|)) \right] \frac{E_{\ell}}{I_n} d\ell. \quad (3)$$

The elliptic spiral function is given by,

$$\underline{\rho} = (\rho_o + a\phi)(K_x \cos \phi \hat{x} + K_y \sin \phi \hat{y}) \quad (4)$$

and the vector $\underline{\rho}$ therefore locates a point on the spiral contour ℓ , with source and field points differentiated by primes, as shown in Fig 1b. K_x and K_y denote spiral stretching constants in the x and y directions respectively and a is the spiral constant.

The vector derivatives in equation (2) are obtained through,

$$\frac{\partial \rho_i}{\partial \ell} = \frac{\partial \rho_i}{\partial \phi} \times \frac{\partial \phi}{\partial \ell} \quad (5)$$

where $i = (x, y)$ and,

$$\frac{\partial \ell}{\partial \phi} = \sqrt{\left(\frac{\partial \rho_x}{\partial \phi}\right)^2 + \left(\frac{\partial \rho_y}{\partial \phi}\right)^2} \quad (6)$$

Substitution of equation (4) in equations (5) and (6) allows equation (2) to be finally written for the elliptical spiral as,

$$E_\ell = \frac{I_n k}{j\omega\epsilon_2 \sin(k\Delta\ell')} \times \left\{ \begin{array}{l} \int_{n-1}^{n+1} k \sin k(\Delta\ell' - |\ell' - \ell_n|) \times G \frac{F_1}{F_2 F_3} \\ + v \cos k(\Delta\ell' - |\ell' - \ell_n|) \frac{\partial}{\partial \ell} (G + II) d\ell' \end{array} \right\} \quad (7)$$

where,

$$F_1 = K_x^2 (a \cos \phi - \rho \sin \phi)(a \cos \phi' - \rho' \sin \phi') + K_y^2 (a \sin \phi + \rho \cos \phi)(a \sin \phi' + \rho' \cos \phi')$$

$$F_2 = \sqrt{\begin{array}{l} a^2 (K_x^2 \cos^2 \phi + K_y^2 \sin^2 \phi) \\ + 2a\rho \sin \phi \cos \phi (K_x^2 - K_y^2) \\ + \rho^2 (K_x^2 \sin^2 \phi + K_y^2 \cos^2 \phi) \end{array}}$$

$$F_3 = \sqrt{\begin{array}{l} a^2 (K_x^2 \cos^2 \phi' + K_y^2 \sin^2 \phi') \\ + 2a\rho' \sin \phi' \cos \phi' (K_x^2 - K_y^2) \\ + \rho'^2 (K_x^2 \sin^2 \phi' + K_y^2 \cos^2 \phi') \end{array}}$$

$v = +1$ for $\ell_{n-1} \leq \ell' < \ell_n$ and $v = -1$ for $\ell_n \leq \ell' \leq \ell_{n+1}$. Since the spiral is segmented in equal values of $\Delta\ell$ in a Galerkin type MoM procedure with integration along $\hat{\ell}$, a root solver or interpolation procedure is required in equation (6) to obtain values of ϕ corresponding to values of ℓ in the numerical integration interval. To facilitate this for the elliptical spiral equation (6) can be written,

$$\ell = \int_0^\phi F_2 d\phi \quad (8)$$

The terms G and II are evaluated using the GPOF technique after reformulation as complex image terms. Since these functions are independent of the spiral contour, their description in [5] is applicable here, and is therefore not repeated. Once the spiral currents have been determined using the MoM, parameters such as input impedance, gain and axial ratio can be evaluated. The far field of the elliptical spiral is given by,

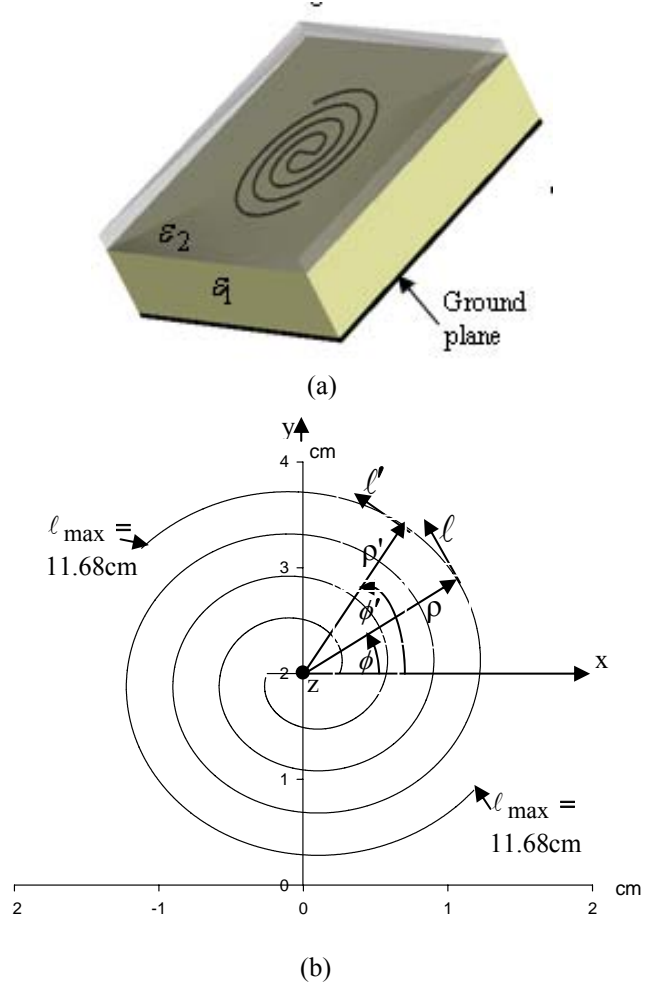


Fig. 1. Spiral geometry.

$$E_\phi = -j30kG_x \frac{e^{-jkR}}{R} \int_{\ell'} \frac{A_1}{F_3} e^{-jk\rho A_3} I_{\ell'} d\ell' \quad (9)$$

$$E_\theta = -j30k(\cos \theta G_x - \sin \theta G_z) \frac{e^{-jkR}}{R} \times \int_{\ell'} \frac{A_2}{F_3} e^{-jk\rho A_3} I_{\ell'} d\ell' \quad (10)$$

where

$$A_1 = a(-K_x \cos \phi' \sin \phi + K_y \sin \phi' \cos \phi) + \rho(K_x \sin \phi' \sin \phi + K_y \cos \phi' \cos \phi) \quad (11)$$

$$A_2 = a(K_x \cos \phi' \cos \phi + K_y \sin \phi' \sin \phi) - \rho(K_x \sin \phi' \cos \phi - K_y \sin \phi \cos \phi') \quad (12)$$

$$A_3 = \sin \theta(K_x \cos \phi' \cos \phi + K_y \sin \phi' \sin \phi), \quad (13)$$

and θ is the spherical co-ordinate angle from the z-axis in Fig. 1, and again $G_{x,z}$ are defined in [5].

To optimise the parameters of the designs considered here, the Optimisation using Marginal Distributions (OMD) algorithm is used [9]. Briefly, with reference to Fig. 2, OMD is a stochastic search algorithm that uses statistical information derived from the optimisation process to guide its search for an optimum design.

In this work, seven parameters are optimised to produce an elite set containing candidates with axial ratios closest to unity and high gains over wide bandwidths, as evaluated using the MoM code. These parameters are: substrate and superstrate thickness and permittivity,

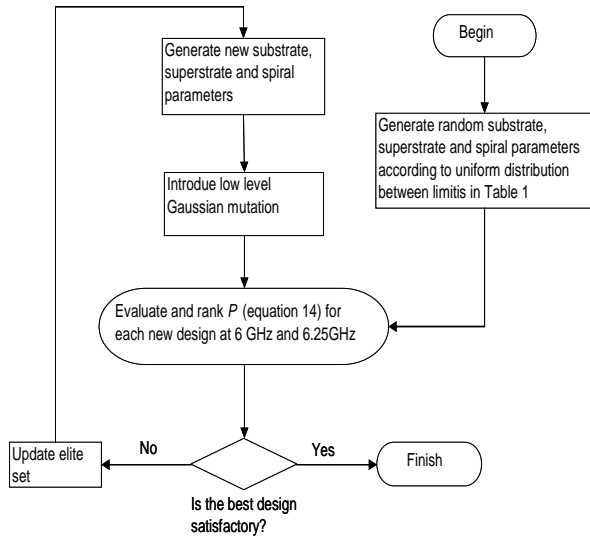


Fig. 2. OMD flowchart.

$B_1, B_2, \varepsilon_1, \varepsilon_2$ respectively; spiral constant, stretching constant and maximum winding angle a, K_x, ϕ_m respectively ($K_x = 1$). The seven marginal probability density functions $P(B_1), P(\varepsilon_1), P(B_2)$. etc associated with the elite set have peaks corresponding to concentrations of elite candidates in the search space. When it comes to generating a new antenna design, the thickness of the substrate, B_1 for example will be chosen using a random number generator with probability

density function matching $P(B_1)$. A similar procedure will then be used to choose the other six parameters. In this way it is ensured that the values chosen for the new population are most likely to be close to the more often occurring values of the elite set. The performance of each member of the new population is then evaluated using the fitness criterion,

$$P = |G_m - G| + |A_R - 1| + |R_1 - R_2| + |X_1 - X_2| \quad (14)$$

where G_m is greater than the highest anticipated gain, G denotes antenna gain, A_R axial ratio, and R, X the input resistance and reactance at the two evaluation frequencies. The separation of these frequencies is judiciously chosen to potentially increase the bandwidth while not being so large as to compromise the optimised gain and axial ratio. Candidates are then ranked in order of lowest P factor, with superseded elite set members being removed so as to maintain a constant elite set membership.

III. RESULTS

Table 1 details the imposed limits on the optimisation parameters, which were chosen heuristically to obtain the best chance of good performance for a manageable size. For instance, if the substrate permittivity were allowed to increase further, surface wave loss could make the antenna less efficient. Table 2 shows the final optimised values of these parameters.

Table 1. Optimisation limits.

	B_1 /cm	B_2 /cm	ε_{r1}	ε_{r2}	a cm /rad	ϕ_m	Ky
Upper limit	0.5	0.01	2	2	0.07	8	1.1
Lower limit	1.5	0.5	5	5	0.11	17	2.

Table 2. Optimised spiral parameters ((a) with superstrate, (b) without superstrate).

	B_1 /cm	B_2 /cm	ε_{r1}	ε_{r2}	a cm /rad	ϕ_m	Ky
(a)	1.47	0.33	4.2	4.29	0.103	11.98	1.24
(b)	0.74	-	3.1	-	0.088	10.95	1.84

These were obtained by running the MoM code with 25 curved segments per arm (to ensure convergence) at 6GHz and 6.25GHz, using a population and elite set size of 40 candidates over 7 generations. A single run of the MoM code took 2.5 mins on a Pentium 4 2.8GHz processor, so that a complete optimisation run took 23 hours. For each spiral $\rho_o = 0.25$ cm and the wire radius is 0.03 cm.

Designs were optimised both with and without a superstrate to allow comparisons of the best performance one might expect using otherwise identical optimisation criteria. Figure 3 shows impedance bandwidth plots, and the spiral with superstrate has much more uniform input impedance. Our MoM code is also compared with a control using CST Microwave Studio [10].

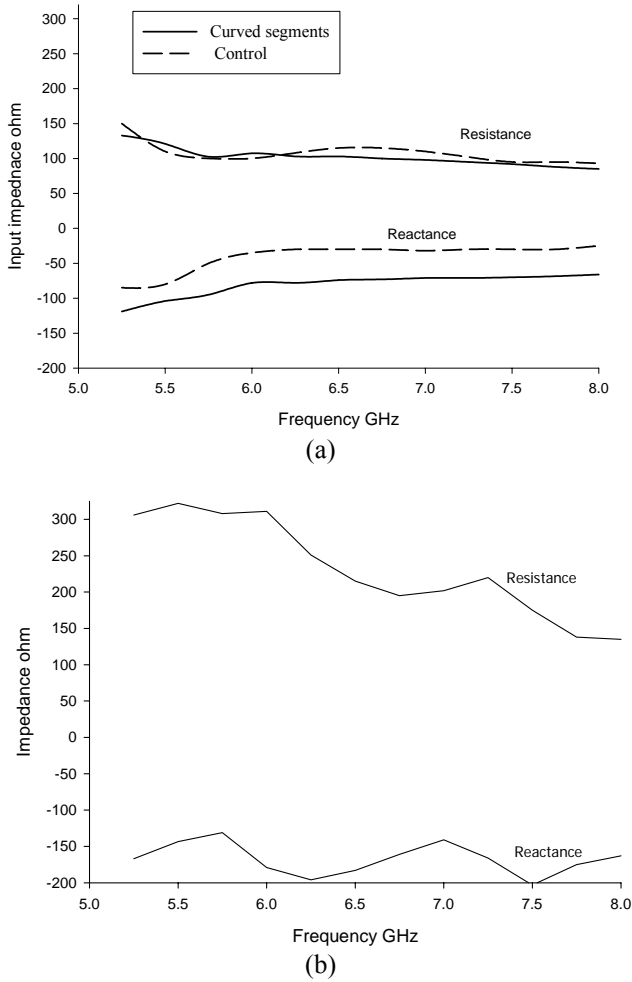


Fig. 3. Input impedance of optimised spiral in Table 2; (a) with and (b) without superstrate.

The convergence of input impedance with number of curved segments is shown in Fig. 4 and a main advantage of using curved segmentation is the more rapid convergence obtained compared with linear segmentation.

The current distribution along a spiral arm in Fig. 5 is predominantly a travelling wave, although interference between the incident and reflected waves is apparent towards the end of an arm with the superstrate, where relative magnitudes are similar.

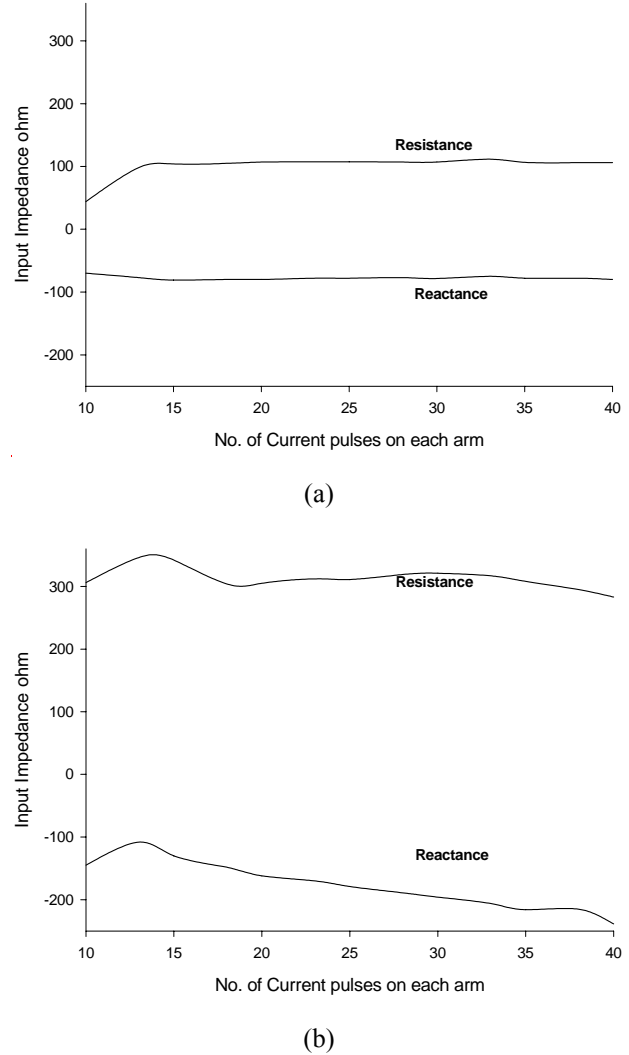
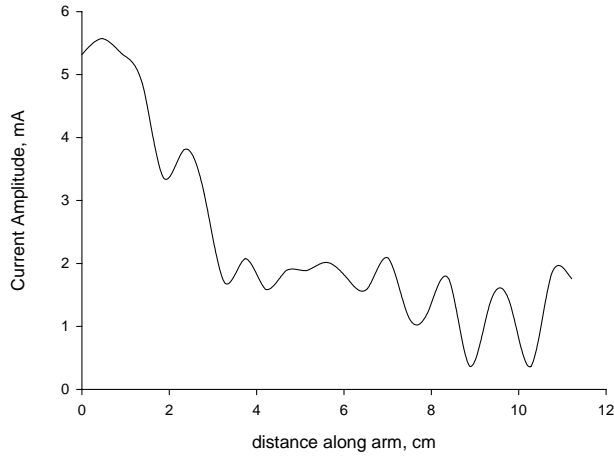


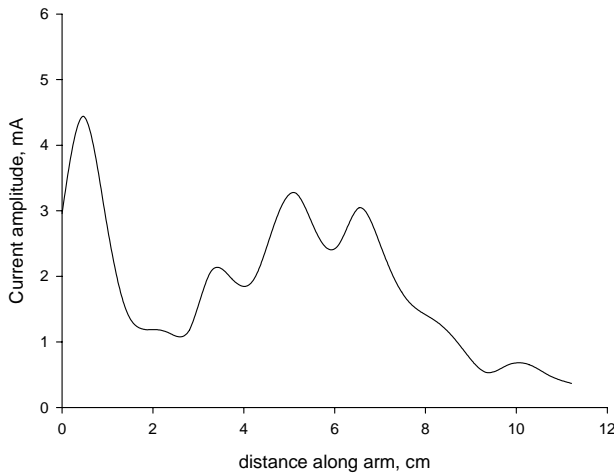
Fig. 4. Convergence of input impedance of spiral with number of curved basis functions; (a) with and (b) without superstrate at 6 GHz.

Radiation patterns are shown in Fig. 6, where the peak values of E_θ and E_ϕ are similar, for the spiral with a superstrate, suggesting a low axial ratio and good circular polarization, although the time phasing also needs to be considered. Note also the narrower beam width in the $\phi = 90^\circ$ cut, especially without a superstrate, corresponding to the direction of the major axis of the ellipse along the y axis, which indicates how the pattern can be shaped in orthogonal planes using elliptical spirals.

The plots in Fig. 7 confirm a successful design with low axial ratio and useful gain. As can be seen from the summary Table 3, the spiral with superstrate has slightly higher gain and significantly wider axial ratio bandwidth compared with the printed spiral.

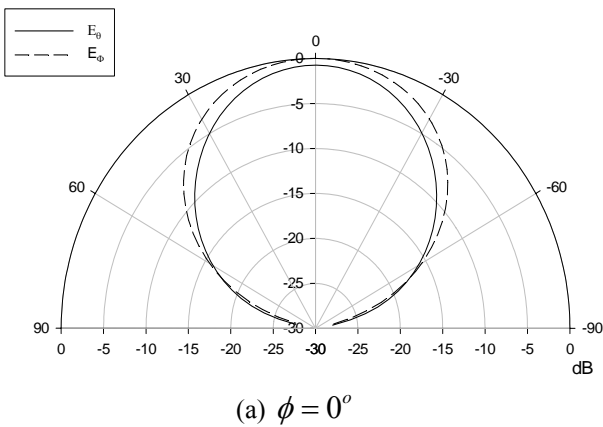


(a)

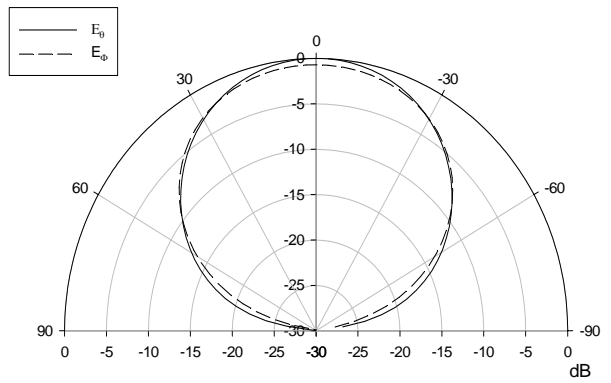


(b)

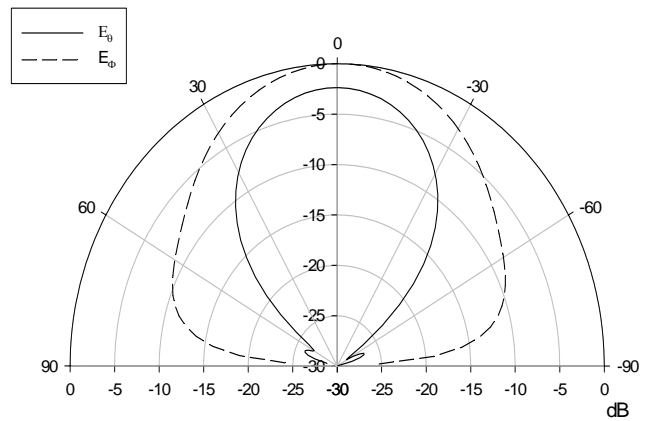
Fig. 5. Current distribution along optimised spiral arm; (a) with and (b) without superstrate at 6 GHz.



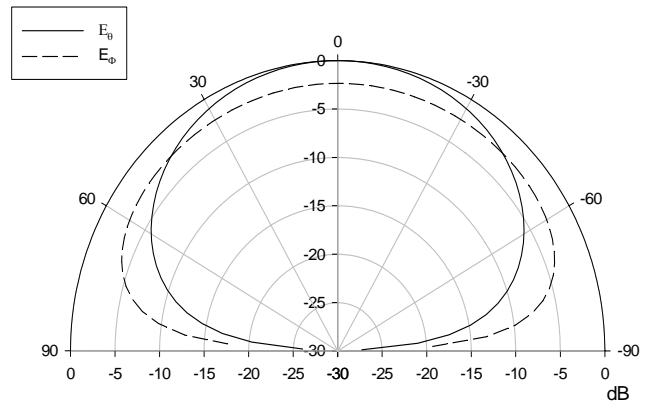
(a) $\phi = 0^\circ$



(b) $\phi = 90^\circ$



(c) $\phi = 0^\circ$



(d) $\phi = 90^\circ$

Fig. 6. Radiation patterns as a function of θ of optimised spiral lying in x - y plane with major axis along y direction; (a) and (b) with superstrate, (c) and (d) without superstrate at 6 GHz.

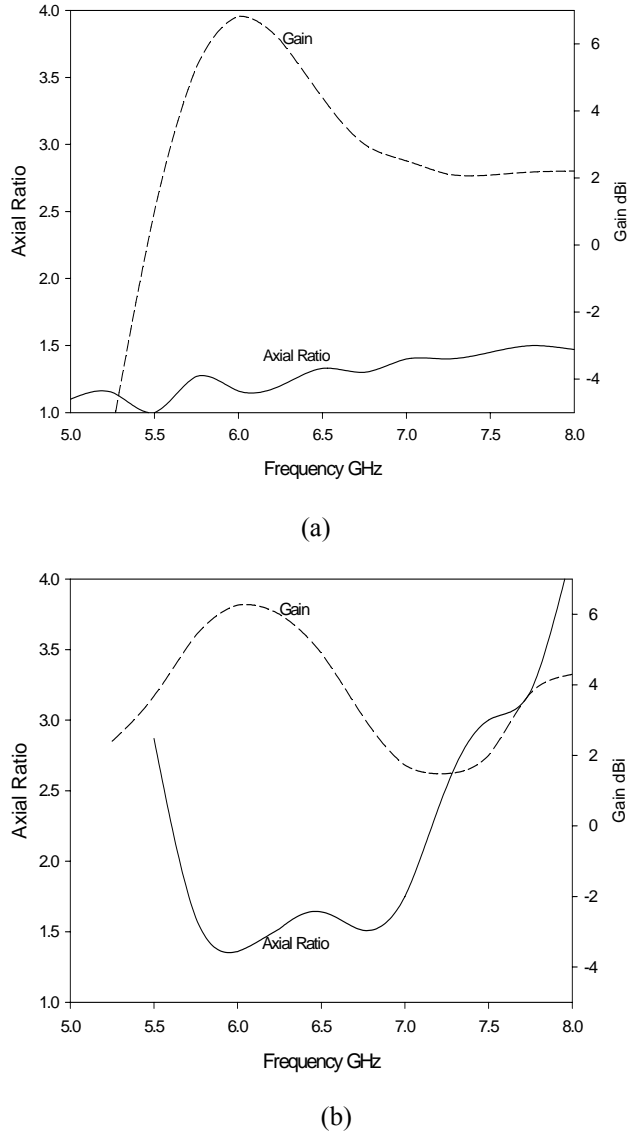


Fig. 7. Axial ratio and gain of optimised spiral (a) with and (b) without superstrate.

Table 3. Optimised spiral performance ((a) with superstrate, (b) without superstrate).

	Gain dBi	3dB Bandwidth	
		Gain	Axial ratio
(a)	6.8	16%	> 46%
(b)	6.2	20%	25%

IV. CONCLUSION

A printed spiral with a dielectric superstrate has been optimised for gain, axial ratio and bandwidth, by varying four environmental and three spiral parameters, using original efficient MoM code under an OMD optimiser.

The benefits of the superstrate are a significant broadening of the impedance and axial ratio bandwidths with, a slight increase in gain, and protection of the spiral element. These must be considered against the disadvantage of increased bulk or weight of the antenna with the 0.33cm thick superstrate. The elliptical spiral design gives a further benefit of differential pattern shaping in the two principal planes.

REFERENCES

- [1] K. Hirose and H. Nakano, "An eccentric spiral antenna printed on a dielectric substrate," *IEEE Antennas Propag. Soc. Int. Sym.*, 1, pp. 190-193, 1995.
- [2] S. K. Khamas and G. G. Cook, "Moment method analysis of printed wire spirals using curved piecewise sinusoidal subdomain basis and testing functions," *IEEE Trans. Antennas Propagat.*, vol. 45, no. 6, pp. 1016-1022, 1997.
- [3] S. K. Khamas and G. G. Cook, "Moment method analysis of printed eccentric spiral antennas using curved segmentation," *IEE Proc. Microwave Antennas Propagat.*, vol. 146, no. 6, pp. 407-410, 1999.
- [4] R. M. Edwards, G. G. Cook, S. K. Khamas, R. J. Aidley, and B. Chambers, "Design of a circularly polarised printed spiral antenna using a dual objective genetic algorithm," *Electron. Lett.*, vol. 34, no. 7, pp. 608-609, 1998.
- [5] S. K. Khamas and G. G. Cook, "Design of a printed spiral antenna with a dielectric superstrate using an efficient curved segment moment method with optimisation using marginal distributions," *IEE Proc. Microwave Antennas Propagat.*, vol. 151, no. 4, pp. 315-320, 2004.
- [6] Y. L. Chow, J. J. Yang, D. G. Fang, and G. E. Howard, "A Closed form spatial Green's function for the thick microstrip substrate," *IEEE Trans. Microw. Theory Tech.*, vol. 39, no. 3, pp. 588-592, 1991.
- [7] M. Aksun, "A robust approach for the derivation of closed-form Green's functions," *IEEE Trans Microw. Theory Tech.*, vol. 44, no. 5, pp. 651-658, 1996.
- [8] R. M. Edwards, S. K. Khamas, and G. G. Cook, "Design of printed eccentric spiral antennas using genetic algorithm optimisation," *IEE Conference on Antennas and Propagat.*, York, Conference Proceedings, 461, pp. 375-379, 1999.
- [9] P. L. Starke and G. G. Cook, "Optimisation of an unequally spaced dual-band printed base station antenna array using a marginal distribution technique," *IEE Proc. Microwaves, Antennas Propagat.*, vol. 49, no. 4, pp. 211-217, 2002.

[10] CST Reference Manual. Darmstadt: Computer Simulation Technology, 2006.



Salam Khamas is a lecturer in the Dept. of Electronic and Electrical Engineering, University of Sheffield. He has worked in Antennas since 1988 when he designed the first high temperature superconducting dipole antenna. A patent was awarded and a prize winning paper was published on that work. Since then he has continued to work on various aspects of antenna modelling and design, which resulted in approximately 27 published journal papers. His research interests include computational electromagnetics, superconducting antennas, conformal antennas, frequency independent antennas, array design and magnetic resonance imaging.



Greg Cook is a Reader in electromagnetics in the Dept. of Electronic and Electrical Engineering at Sheffield University. His research interests include microwave holographic antenna metrology and imaging, superconducting antennas and electromagnetic modelling, specifically using novel Method of Moments software to analyse printed geometries such as spirals for cellular mobile communications. Latterly he has worked on electromagnetic interactions with biological tissue, and designed TEM cell dosimetry apparatus using original Finite Difference Time Domain code to investigate stress response mechanisms in human tissue. Research is also being conducted in Magnetic Resonance Imaging, to track in-vivo neuronal impulses as perturbations in the gradient field.